Available online at www.sciencedirect.com

ScienceDirect

Energy Procedia 92 (2016) 130 – 137

Energy Procedia

6th International Conference on Silicon Photovoltaics, SiliconPV 2016

Defects in multicrystalline Si wafers studied by spectral photoluminescence imaging, combined with EBSD and dislocation mapping

Torbjørn Mehl[a,*], Marisa Di Sabatino[b], Krzysztof Adamczyk[b], Ingunn Burud[a] and Espen Olsen[a]

[a]*Norwegian University of Life Sciences, NMBU, Universitetstunet 3, 1430 Ås, Norway*
[b]*Norwegian University of Science and Technology, NTNU, Alfred Getz vei 2B, 7491 Trondheim, Norway*

Abstract

Defect related sub-band gap luminescence emissions due to Shockley-Read-Hall recombination in mc-Si wafers have been investigated with spectral photoluminescence imaging, combined with electron backscatter diffraction and dislocation mapping, for p- and n-type wafers, with and without intentionally introduced Fe. The well-known emission with energy 0.807 eV (D1) is found to be correlated with heavily dislocated areas of the wafers with emissions emanating from the immediate vicinity of the defects. A less studied emission with energy centered around 0.7 eV (D07) may be the product of two emissions and is found to exhibit very different characteristics in a boron-doped wafer intentionally contaminated with Fe than in the other samples. There is reason to believe that a radiative recombination pathway with characteristic photons with energy 0.694 eV is present in this sample due to interstitial iron, Fe_i, while the D3/D4 (0.938 eV/1.00 eV) emission pair is related to the FeB complex.

Peer review by the scientific conference committee of SiliconPV 2016 under responsibility of PSE AG.

Keywords: Silicon; Defects; Solar cells; Photoluminescence; Iron.

* Corresponding author. Tel.: +47-67231645.
E-mail address: torbjorn.mehl@nmbu.no

Peer review by the scientific conference committee of SiliconPV 2016 under responsibility of PSE AG.
doi:10.1016/j.egypro.2016.07.043

1. Introduction

Material defects in silicon wafers for PV applications lead to a significant reduction of the efficiency of the final solar cells due to a decrease of the carrier lifetime. Spectral photoluminescence imaging (SPL) is a technology that can reveal new knowledge on the shape and structure of radiative recombination active centers originating from crystal imperfections in the silicon wafers [1]. It is a non-destructive and non-contact method used on full size wafers and solar cells.

The SPL method combines two established methods for recording photoluminescence (PL) from silicon wafers and solar cells, PL imaging [2] and PL spectroscopy [3]. PL imaging gives the spatial distribution of defect related luminescence (DRL) integrated over the spectral range, and selected spectral regions can be obtained by mounting different filters prior to the recording. PL spectroscopy, on the other hand, gives the whole DRL spectrum, but has no spatial resolution. Therefore, selection of location is essential and required prior to scan. SPL overcomes these limits and extracts the advantages of both methods. For each spatial pixel in the image, the full PL spectrum is stored. From the stored image, it is possible to select a variety of energy levels or specific regions for more detailed studies.

In order to obtain information on origin and nature of the selected regions from the spectral imaging measurements, it is necessary to correlate the images with other complementary material characterization techniques. In this work, spectral imaging has been combined with electron backscatter diffraction (EBSD) and dislocation mapping to study correlations between radiative recombination active centers, dislocation density and crystal orientation.

Multivariate curve resolution (MCR) has been utilized in this study. It is a method in multivariate statistics that decomposes the measured data matrix D into a number of representative score matrices S^T (images in our case) with corresponding loading vectors C that represent the weight of each variable (energy) used to obtain the score image. In the present application, the loading vector can be looked upon as a deconvolution of the numerous complex signals in the data set. The score images yield the spatial distribution of each of the emissions seen in the loadings. An error matrix E represents the difference between the recorded and the simulated signal, and is minimized using an alternating least squares (ALS) algorithm [4]. MCR can be represented mathematically by Eq. (1)

$$D = CS^T + E \tag{1}$$

2. Material and method

The samples investigated were multicrystalline silicon wafers made in a pilot scale, cylindrical furnace (12 kg charge). The dimensions were originally 125x125 mm^2 with thickness of approximately 200 μm. Three samples were investigated in this study: sample A: p-type, boron-doped; sample B: p-type boron-doped with Fe added to the charge; and sample C: n-type phosphorous doped with Fe added.

First, the samples were analyzed using spectral photoluminescence. The SPL setup comprised a hyperspectral camera (sensitivity range 900 - 2500 nm), an excitation source (808 nm, 2W/cm^2 laser) and a liquid N_2-based cryogenic sample holder (77K - RT). In this study, the spatial resolution was 100 μm and the temperature set to 90K.

The samples were then polished down to 1 μm and analyzed by JEOL JSM 840 SEM equipped with NORDIF EBSD detector for mapping of grain orientation and grain boundary types. The samples were etched with Sopori etchant and the dislocation density measured by an automated dislocation scanning system (PVScan by GT Solar).

To study the impact of etching on the PL properties, SPL scans were again performed. The spectra were processed by MCR using the software package MatLab equipped with the MIA_Toolbox and PLS_Toolbox extension.

3. Results and discussion

The total PL spectrum from sample A, p-type wafer, is shown in Figure 1. The peaks on the graph correspond with the defect luminescence bands D1 – D4 [5], D07 [6] and band-to-band recombination PL signal (BB-PL). An image of the integral of all DRL signals in the interval 0.5 – 1.0 eV, equal to what one would get from established PL imaging, is shown in Figure 1 top right. From such an image, it is almost impossible to distinguish between different types of defects. To illustrate the possibilities of the SPL method, images of the defect related emissions D07 (0.694 eV), D1 (0.807 eV) and D4 (1.00 eV) are shown in Figure 1 bottom right, respectively. Their spatial distribution is clearly not correlated.

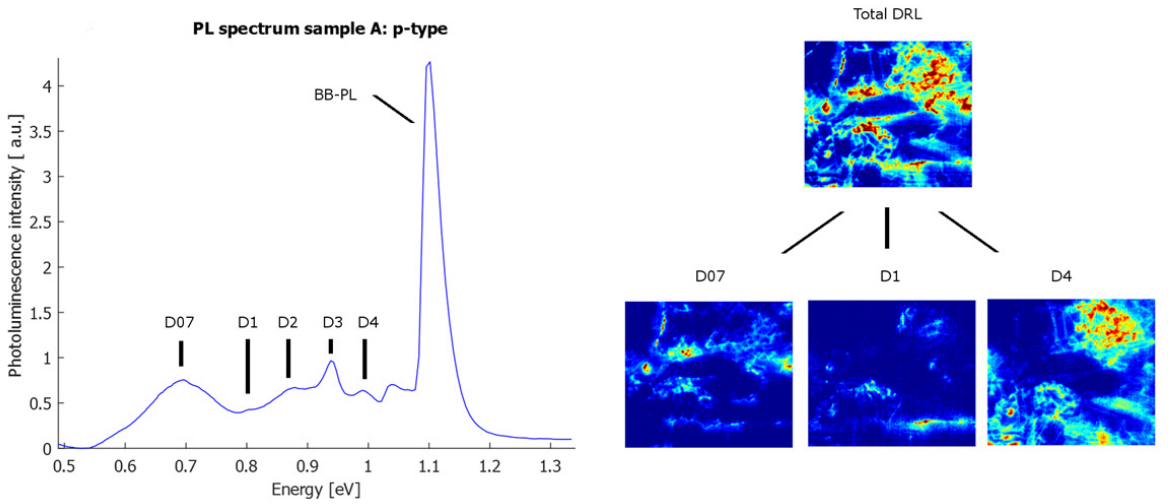

Fig. 1. Left: Accumulated luminescence emission spectrum from p-type boron-doped mc-Si wafer. Top right: PL image of all defect related luminescence in the interval 0.5 eV to 1.0 eV. Bottom: PL images of some selected defect signals; D07 (0.694 eV, left), D1 (0.807 eV, middle) and D4 (1.00 eV, right).

3.1. Spectral and spatial distribution of D07 signal

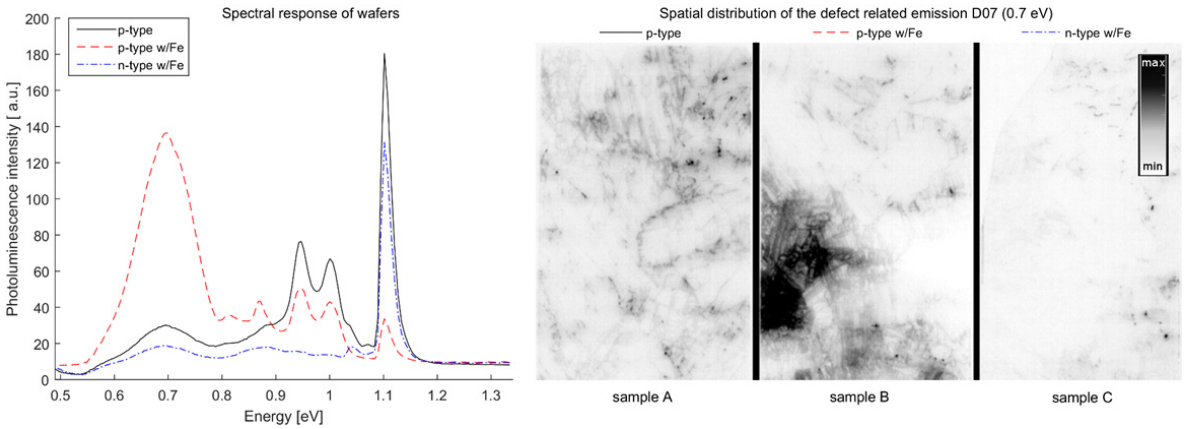

Fig. 2. Left panel: Accumulated luminescence emission spectrum from the three types of wafers, measured at 90K. Right panel: Spatial distribution of the defect related emission D07 (0.7 eV) in the three different wafers. Left image: Sample A, p-type with no added Fe; Middle image: Sample B, p-type with added Fe; Right image: Sample C, n-type with added Fe. The images are inverted in order to better visualise the emission signals (shown in black).

The total spectra from all the samples investigated and the distribution of the D07 signal are shown in Figure 2. All spatial distribution images are an integral over the interval from the spectral response center peak ± 0.05 eV. It is evident from Figure 2 that the D07 signal is found in all the samples. The n-type sample shows a notable lower signal strength, though. The boron-doped sample with Fe intentionally added exhibits significantly higher signal. This may indicate that the D07 emission is associated with Fe. The D07 signal is notably different in the two p-type samples. In sample A and C, the signal occurs as spot-like features or, seemingly, along grain boundaries. In sample B, however, the signal appears as distributed within the grains as well as along the boundaries and in spots.

In Figure 3, a spectrum from a bright, distributed D07 intra-grain area in sample B is compared with a spectrum from a bright spot. The two D07 signals have both different spatial distribution and also slightly different spectral behaviors, indicating that the two signals have different origins. In the extended areas, the center peak energy is at 0.694 eV with a marked peak energy. This signal with distributed occurrence appears strong in the intra-grain areas of the p-type wafer intentionally contaminated with Fe. In other areas, it is weak or not present. The signal emanating from the spots has a slightly higher center energy of 0.716 eV, found in all samples. This signal appears blunt on top.

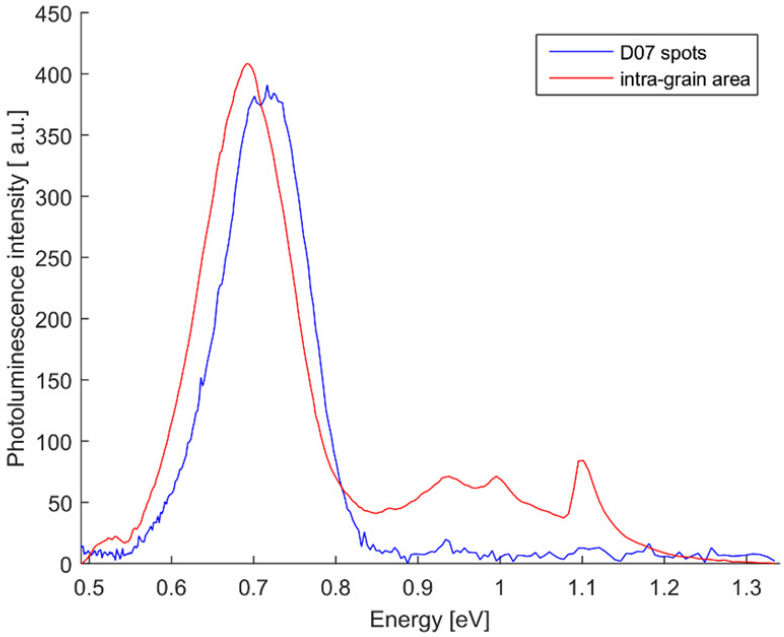

Fig. 3. Spectra from distributed D07 intra-grain area (red) signal versus D07 spot (blue) in sample B, p-type with Fe added. The intra-grain signal shows correlation with the D3/D4 and BB-PL signals while this is absent in the spot-like emission.

3.2. Dislocations

In order to find correlations between different DRL signals, crystal structure and dislocations, the PL images were visually compared with EBSD and PVScan, respectively, see Figure 4. The distribution of the emission signal D07 (0.694 eV) was compared for the three samples. For all three wafers (only sample B shown here), D07 correlate with grain boundaries, especially Σ9, Σ27 and random GB.

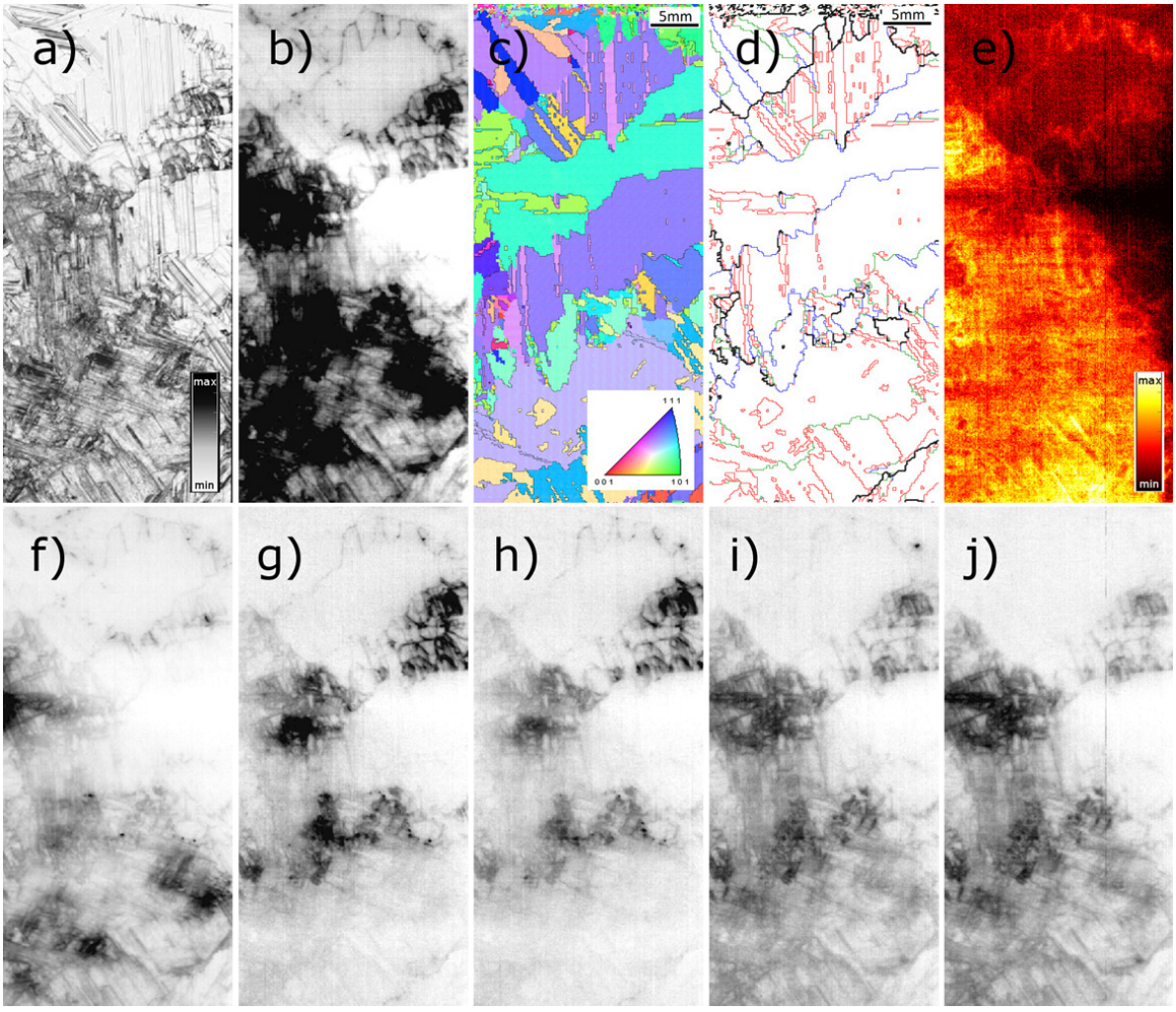

Fig. 4. Spatial distribution of features in sample B; p-type boron-doped mc-Si wafer with addition of Fe. (a) Dislocation mapping, (b) DRL image (integral of signal (0.5 – 1.0 eV), (c) grain orientation, (d) grain boundary types. Coincident site lattice (CSL) grain boundary type Σ3 in red, Σ9 in green, Σ27 in blue and random GB in black. (e) BB PL (1.10 eV). (f) Spatial distribution of D07 (0.694 eV), (g) D1 (0.807 eV), (h) D2 (0.875 eV), (i) D3 (0.938 eV) and (j) D4 (1.00 eV).

For the p-type wafer enriched with Fe there is an additional signature of the spatial distribution of the emission signal. There seems to be a strong D07 emission in regions with high dislocation density for this sample (Figure 4 (f) vs (a)). Since the wafer is enriched with Fe, this could possibly be due to Fe-B pairs or interstitial iron (Fe_i).

When comparing images of the radiative photoluminescence signals D1 (0.807 eV) and D2 (0.875 eV) with dislocation maps, the spatial distribution of D1 and D2 correlates and the regions with D1 and D2 emissions have high dislocation density, as shown for a selected part of the p-type wafer enriched with Fe. The D1 and D2 signals also seem to be correlated with the crystal directions. Grain boundaries show no correlation with D1 and D2. In Figure 4, it seems to be a correlation with random GB, but the signal have slightly different energy, see section 3.3 below.

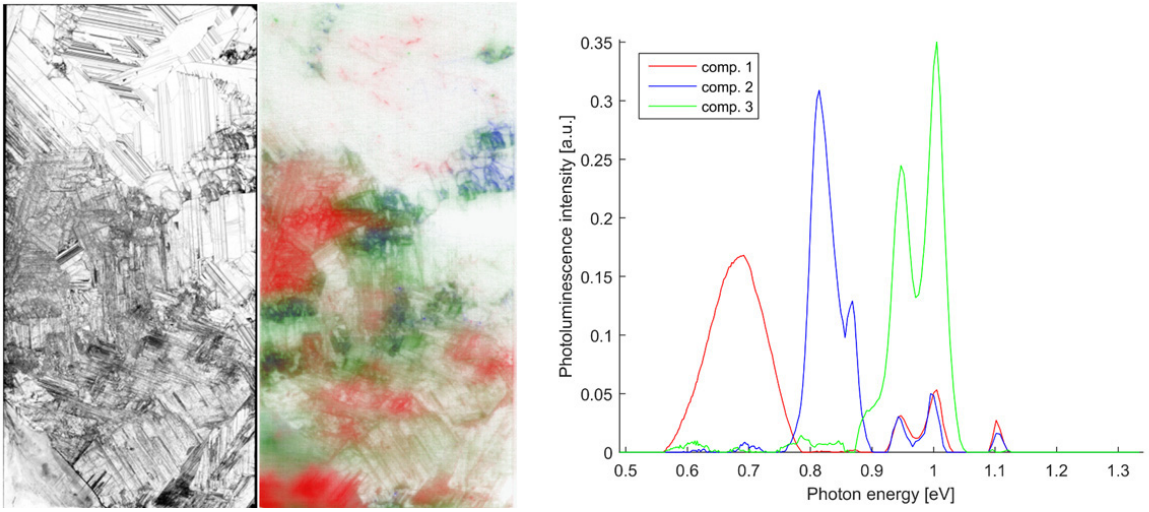

Fig. 5. Dislocation density of sample B beside image and graph of three components from an MCR analysis. It is correlation between high dislocation density and spatial distribution of the components. Comp. 1 (red) correspond to D07 with weak signals of D3 and D4. Comp. 2 (blue); D1 and D2 with weak D3 D4. Comp. 3 (green): D3 D4.

The spatial distribution of D3 and D4 signals seems to correlate and the two signals emits from areas with high dislocation density. The dislocation density patterns of D1/D2 and D3/D4 looks different. Future studies will have to be done to distinguish these dislocation density patterns. It also seems that D1/D2 have a higher negative impact on the band-to-band luminescence than D3/D4, cf. [7]. The D3/D4 signals also seem to be present, but weak, in areas with D1/D2. To separate the different signals and group them spectrally and spatially, an MCR analysis is conducted on the hyperspectral image.

The result from an MCR analysis is depicted in Figure 5. It groups the DRL into three components. Component 1, red in Figure 5, exhibit a spectrum with center peak energy 0.69 eV but also to relatively weak peaks at 0.94 eV (correspond to D3) and 1.00 eV (D4). This indicate that the 0.694 eV and D3/D4 are of FeB / Fe_i origin. The different states give rise to the different signals. Graff [8] states that FeB leads to a shallow level in the band gap of Si at E_V +0.1 eV. This is in accordance with the D4 signal at 1.00 eV emanating from carrier recombination from E_C to E_T. It is widely reported that the D3/D4 signal is a primary mechanism with its associated replica. If this is the case, recombination through this level may give raise to both these signals. Interstitial Fe_i is, on the other hand, reported to introduce a level at E_V +0.39 eV. This is in accordance with at least one of the D07-related signals (Fig. 3) to be associated with Fe_i. This will be investigated further in an upcoming paper.

The state of the binding in Fe-containing complexes in the Si structure has been subject to much debate. Within one of the proposed models, covalent bonding between Fe and the Si atoms nearest to the substitutional B plays a significant role and suggestions are made that there are no direct covalent bond between the Fe and the B [9]. We may speculate that if this is the case, the actual substitutionally placed element may not be crucial in the Fe-containing complex. The same mechanisms may therefore come to play for other elements than B with similar bonding characteristics in the Si lattice. This may explain the occurrence of a D3/D4-like emission pair in Fe-doped n-type Si. This calls for further fundamental studies.

Component 2, blue in Figure 5, has center peaks energy levels corresponding to D1 and D2 with weak D3 and D4. Component 3, green in Figure 5, has center peaks corresponding to D3 and D4. The two MCR-components spectra correspond to previous studies [10,11], where the recombination active defects were grouped in two types; Here, component 2 corresponds to Type B and component 3 to Type A, a denomination introduced by Lausch et al. [11]. Type A defects have been correlated with iron impurities [11].

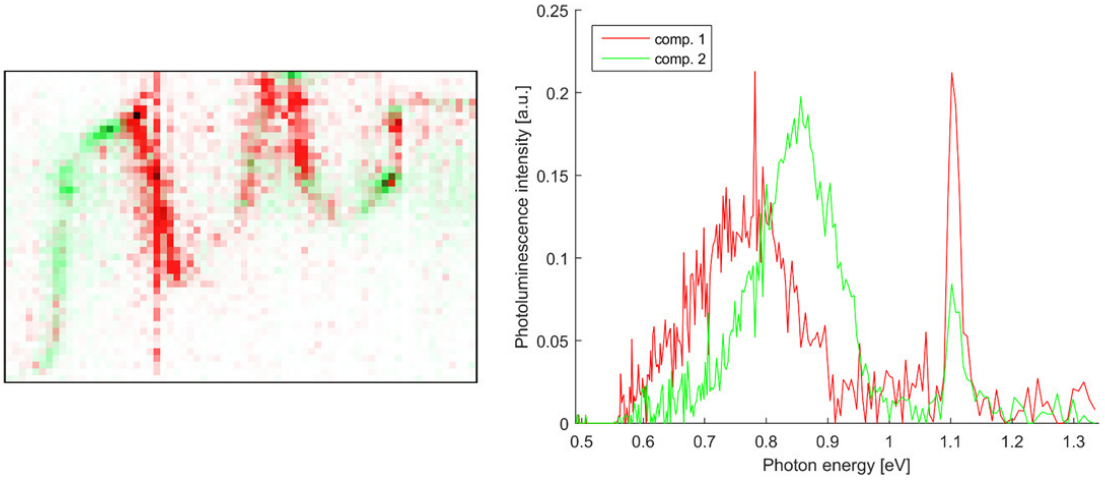

Fig. 6. MCR analysis of area with random GB, obtained from the top part of sample B, as depicted in Figure 4. DRL with center peak energy levels of 0.78 and 0.85 eV and BB PL-signal.

3.3. Red zone

In red zones and other areas with high metallic impurities of multicrystalline silicon ingots, higher Band-to-Band PL-signals have been observed in grain boundaries and dislocation clusters [12]. The internal gettering processes during solidification, will diffuse iron near primary grain boundaries into the boundary regions and effectively locking them there [13]. The depleted region near the grain boundaries will have higher lifetime and thereby higher BB PL-signal than the surroundings. The strongest internal gettering effect has been observed at Random GB [13]. In the p-doped sample w/Fe in Figure 4, we observe a weak BB PL-signal at Random GB, and also DRL of different energy levels. Due to spatial resolution of 100µm, it is not possible to perceive if the BB PL-signal emit from the grain boundary or from adjacent areas. MCR analysis is done on an area obtained from the top part of sample B. The algorithm divide the DRL into two different components, with center peak energies of 0.78eV and 0.85eV respectively. BB is present in both. Figure 6 shows their spatial distribution and radiative spectrum.

4. Conclusion

In this study, we have used spectral photoluminescence imaging to determine spectral- and spatial distribution of radiative active defects in multicrystalline silicon wafers. Combined with EBSD and dislocation mapping, we have found correlations between different DRL signals, and between DRL and dislocation density. There is a spatial correlation between D1 and D2, and between D3 and D4, respectively. Moreover, D1/D2 and D3/D4 appear in different distinct dislocation areas. By applying MCR analysis, the D1/D2 and D3/D4 have been linked to previously studied Type A and Type B defects, respectively.

The DRL signal around 0.7 eV (D07) may be the product of two emissions, one centered at 0.694 eV and the other at 0.716 eV. The D07 is found to exhibit very different characteristics in a boron-doped wafer intentionally contaminated with Fe than in the other samples. There is reason to believe that a radiative recombination pathway with characteristic photons with energy 0.694 eV is present in this sample due to interstitial iron Fe_i, while the D3/D4 emission pair is related to the FeB complex.

References

[1] Olsen E, Flø AS. Spectral and spatially resolved imaging of photoluminescence in multicrystalline silicon wafers. Appl Phys Lett 2011;99:1.
[2] Trupke T, Bardos RA, Schubert MC, Warta W. Photoluminescence imaging of silicon wafers. Appl Phys Lett 2006;89:044107.
[3] Mudryi AV, Korshunov FP, Patuk AI, Shakin IA, Larionova TP, Ulyashin AG et al. Low-temperature photoluminescence characterization of defects formation in hydrogen and helium implanted silicon at post-implantation annealing. Physica B 2001;308-310:181-4.
[4] Piqueras S, Duponchel L, Tauler R, Juan A. Resolution and segmentation of hyperspectral biomedical images by Multivariate Curve Resolution - Alternating Least Squares. Analytica Chimica Acta 2011;705:1-2:182-192
[5] Drozdov NA, Partin AA, Tkachev VD. Recombination radiation on dislocations in silicon. Sov Phys JETP Lett. 1976;23:597-9.
[6] Flø A, Burud I, Kvaal K, Søndenå R, Olsen E. Distribution of radiative crystal imperfections through a silicon ingot. AIP Advances 2013;3:112120.
[7] Lausch D, Hagendorf C. Influence of different types of recombination active defects on the integral electrical properties of multicrystalline silicon solar cells. J Solar Energy 2015;4:1-9.
[8] Graff K. Metal Impurities in Silicon-Device Fabrication. Springer-Verlag Berlin Heidelberg 2000;ISBN 3-540-64213-7.
[9] Istratov AA, Hieselmair H, Weber ER. Iron and its complexes in silicon. Appl Phys A 1999;69;13-44.
[10] Lausch D, Mehl T, Petter K, Flø AS, Burud I, Olsen E. Classification of crystal defects in multicrystalline silicon solar cells and wafer using spectrally and spatially resolved photoluminescence. J Appl Phys 2016;119:054501.
[11] Lausch D, Petter K, Bakowskie R, Bauer J, Breitenstein O, Hagendorf C. Classification and investigation of recombination-active defect structures in multicrystalline silicon solar cells-recombination models. Proceedings of the 27th EUPVSEC 2012:723-8.
[12] Boulfrad Y, Haarahiltunen A, Savin H, Øverlid EJ, Arnberg L. Enhanced performance in the deteriorated area of mc Si wafers by internal gettering. IEEE J Photovolt 2012;2:479-484.
[13] Knörlien M, Autruffe A, Søndenå R, Di Sabatino M. Internal gettering of iron at extended defects. Energy Procedia 2014;55:539-544.